

# Land-based infrared imagery for marine mammal detection

Joseph Graber<sup>a</sup>, Jim Thomson<sup>ab</sup>, Brian Polagye<sup>a</sup>, Andrew Jessup<sup>b</sup>

<sup>a</sup>Northwest National Marine Renewable Energy Center, University of Washington, Seattle, WA;

<sup>b</sup>Applied Physics Laboratory, University of Washington, Seattle, WA

## ABSTRACT

A land-based infrared (IR) camera is used to detect endangered Southern Resident killer whales in Puget Sound, Washington, USA. The observations are motivated by a proposed tidal energy pilot project, which will be required to monitor for environmental effects. Potential monitoring methods also include visual observation, passive acoustics, and active acoustics. The effectiveness of observations in the infrared spectrum is compared to observations in the visible spectrum to assess the viability of infrared imagery for cetacean detection and classification. Imagery was obtained at Lime Kiln Park, Washington from 7/6/10-7/9/10 using a FLIR ThermoVision A40M infrared camera (7.5-14 $\mu$ m, 37°HFOV, 320x240 pixels) under ideal atmospheric conditions (clear skies, calm seas, and wind speed 0-4 m/s). Whales were detected during both day (9 detections) and night (75 detections) at distances ranging from 42 to 162 m. The temperature contrast between dorsal fins and the sea surface ranged from 0.5 to 4.6 °C. Differences in emissivity from sea surface to dorsal fin are shown to aid detection at high incidence angles (near grazing). A comparison to theory is presented, and observed deviations from theory are investigated. A guide for infrared camera selection based on site geometry and desired target size is presented, with specific considerations regarding marine mammal detection. Atmospheric conditions required to use visible and infrared cameras for marine mammal detection are established and compared with 2008 meteorological data for the proposed tidal energy site. Using conservative assumptions, infrared observations are predicted to provide a 74% increase in hours of possible detection, compared with visual observations.

**Keywords:** infrared, killer whales, *Orcinus orca*, cetaceans, automated detection, marine mammals.

## 1. INTRODUCTION

The primary purpose of this study is to evaluate the efficacy of using infrared (IR) imaging for site characterization and marine mammal monitoring of a proposed tidal energy project in Admiralty Inlet, Puget Sound, Washington. Admiralty Inlet is a known transit point for endangered Southern Resident killer whales (*Orcinus orca*) entering Puget Sound<sup>1</sup>. Current plans for monitoring the site include the use of a passive acoustic detection system based on a network of hydrophones in northern Admiralty Inlet and land-based observers. Land-based infrared detection could augment this approach by providing surface images of killer whales as they pass both day and night. Southern Resident killer whale sightings in Admiralty Inlet are relatively rare with a strong seasonal variation. Further north, at Lime Kiln Park, sightings are nearly a daily occurrence in June and July. Therefore, Lime Kiln Park was chosen to test the efficacy of land-based infrared detection of Southern Resident killer whales.

## 2. INSTRUMENTATION

Infrared and visual imagery were collected at Lime Kiln Park, Washington from 7/6/10-7/9/10. Three cameras in a protective housing were mounted to the railing of the Lime Kiln Park lighthouse (Latitude 48°30'57"N Longitude 123° 9'9"W) at a height of 13 meters above sea level. The cameras were positioned to face west towards Victoria BC with an incidence angle of 72°. The infrared camera used is a FLIR ThermoVision A40M uncooled microbolometer with an 18 mm lens (7.5-14 $\mu$ m, 37° horizontal field of view, 320x240 pixels). The front acrylic glass was removed from the protective housing to avoid attenuation of the IR signal by the glass. Two visual cameras were mounted to the same housing as the FLIR A40M. A Canon VB-C50FSi was used primarily to test the infrared sensitivity of a CCD-based camera for night filming. However, even with the infrared cut filter removed, detection was not possible using the Canon before nautical dawn or after nautical dusk. A Point Grey Research FLEA2 FL2-08S2M was used to collect high resolution black and white images during day recordings.

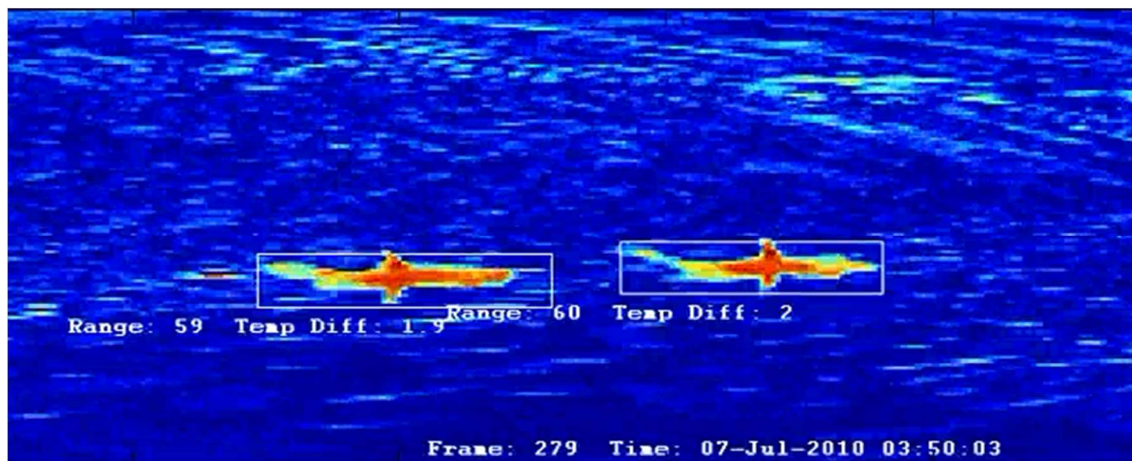
Atmospheric conditions were ideal throughout the field study at Lime Kiln Park with clear skies, air temperatures between 10 and 27 °C, and wind speeds below 4 m/s. During nighttime hours, the relative humidity reached a maximum of 85% and dropped to a minimum of 43% during the warmest part of the day.

### 3. SOUTHERN RESIDENT SIGHTINGS SUMMARY

During the four days of field observations, Southern Resident killer whales (SRKW) passed Lime Kiln Park 11 times. Out of these 11 passes, 8 were recorded as shown in Table 1. During daylight hours the recording on all cameras was initiated by reports of whales in the area by the Orca Network or the Whale Museum’s hydrophone array. Nighttime footage was recorded throughout the night and reviewed the next morning. A “surfacing event”, as reported on Table 1, is counted each time a single whale can be seen above the surface, and a “pass” is a collection of continuous surfaces with no gaps (where no whales can be seen in the footage) longer than 1 minute. Video 1 shows an example of footage recorded at 3:48 on July 7<sup>th</sup>.

Table 1. Summary of SRKW passes observed at Lime Kiln Park from July 6th – July 9th 2010.

Day	Start Time (PDT)	Day/Night	Duration (seconds)	Surfacing events captured on IR	Range (meters)
July 7 <sup>th</sup> 2010	3:48	Night	151	22	42-66
July 7 <sup>th</sup> 2010	3:53	Night	25	3	70-82
July 7 <sup>th</sup> 2010	3:57	Night	44	7	106-111
July 7 <sup>th</sup> 2010	4:59	Twilight	72	23	124-162
July 7 <sup>th</sup> 2010	5:10	Twilight	46	20	52-78
July 7 <sup>th</sup> 2010	11:45	Day	40	4	90-128
July 7 <sup>th</sup> 2010	19:25	Day	33	3	84-97
July 7 <sup>th</sup> 2010	19:46	Day	76	2	97-107



Video 1. Footage of SRKW passing Lime Kiln Park at 3:48 on July 7<sup>th</sup> including the output of the automated detection algorithm. Whales are distinguished from background variations and highlighted with a bounding rectangle. Range and temperature contrast are also displayed. <http://dx.doi.org/doi.number.goes.here>.

### 4. POST-PROCESSING

Whenever possible, infrared image non-uniformities due to sensor drift were removed using the built in, non-uniformity correction (NUC) function. This function mechanically positions an internal blackbody reference in front of the sensor. Camera software then automatically identifies and corrects for non-uniformities in the detector. For daytime recordings, a NUC correction was completed at the start of each pass. Due to limited access to the equipment at night, no NUC corrections were completed during nighttime recordings, resulting in significant noise from sensor drift.

Footage was first reviewed to identify whale sightings. Sections of video with whales were exported from Streams 5 DVR recording software to 16 bit binary format (.raw). The binary files were then read into MATLAB for analysis. Footage of whales was separated into sections of 3 minutes or less (<1350 frames) to enable efficient processing. To identify stationary pixels (due to sensor or lens drift), the mean image was calculated by taking the mean pixel value over all frames within each section. The mean image was then removed from each frame, resulting in an image corrected for drift in the mean. Care was taken to ensure each section of footage has at least 200 frames without whales, so the mean image is not significantly biased by the temperature increase associated with whales surfacing. The pixel value of the corrected frames was then translated from “counts” (cts) associated with the FLIR’s raw signal to temperature contrast (°C) by using the calibration equation<sup>2</sup>.

$$\Delta T = cts/95.2 \tag{1}$$

As shown in Figure 1, the dorsal fin, blow, and body were all distinguishable in the recorded infrared footage. Of these three potential detection targets, the dorsal fin is the only one with a fairly predictable relative angle to the sea surface. Although the angle between the fin and sea surface varies from fin to fin, they remain relatively close to 90°.

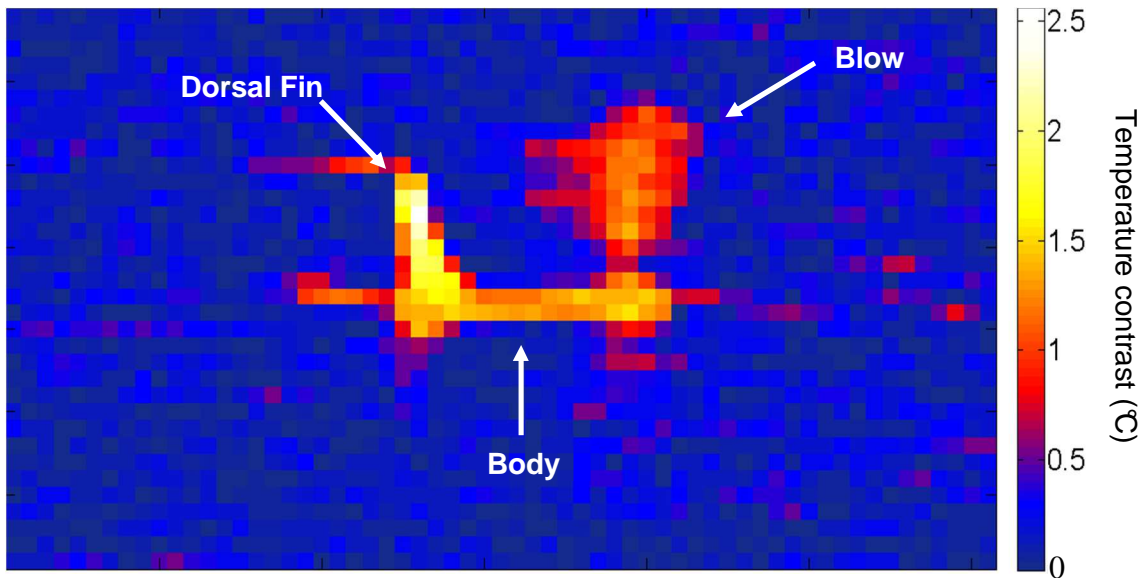


Figure 1. Infrared image of potential targets for cetacean detection. Color map has been adjusted to enhance visual contrast. Color bar shows temperature contrast from the sea surface mean (°C).

Dorsal fins were identified during a second review of footage containing whales. The location of each fin is defined by the vertices of a bounding triangle. The accuracy of each bounding triangle was then rated. A rating of “1” indicates that a dorsal fin is clearly distinguishable and the bounding triangle fits the fin well. A rating of “2” indicates that at least a portion of the dorsal fin is distinguishable and the bounding triangle identifies that portion. A rating of “3” indicates that the dorsal fin could not be clearly distinguished, either from the sea surface or the rest of the whale’s body.

For large incidence angles ( $\theta_{sea} > 60$ ), the angle from the camera to a protruding dorsal fin is near nadir. Assuming the dorsal fin is covered with a film of sea water, it would be expected to have similar emissivity properties as that of water. The estimated range of emissivities for the sea surface and dorsal fin are shown in Figure 2. The fin will have an emissivity near unity while the emissivity of the sea surface decreases rapidly above 60° incidence angle. As the emissivity of the sea surface decreases, more of the received signal depends on reflection from the sky. Since the emissivity of a protruding fin remains fairly constant, the temperature contrast between the fin and the surrounding water is expected to increase with incidence angle.

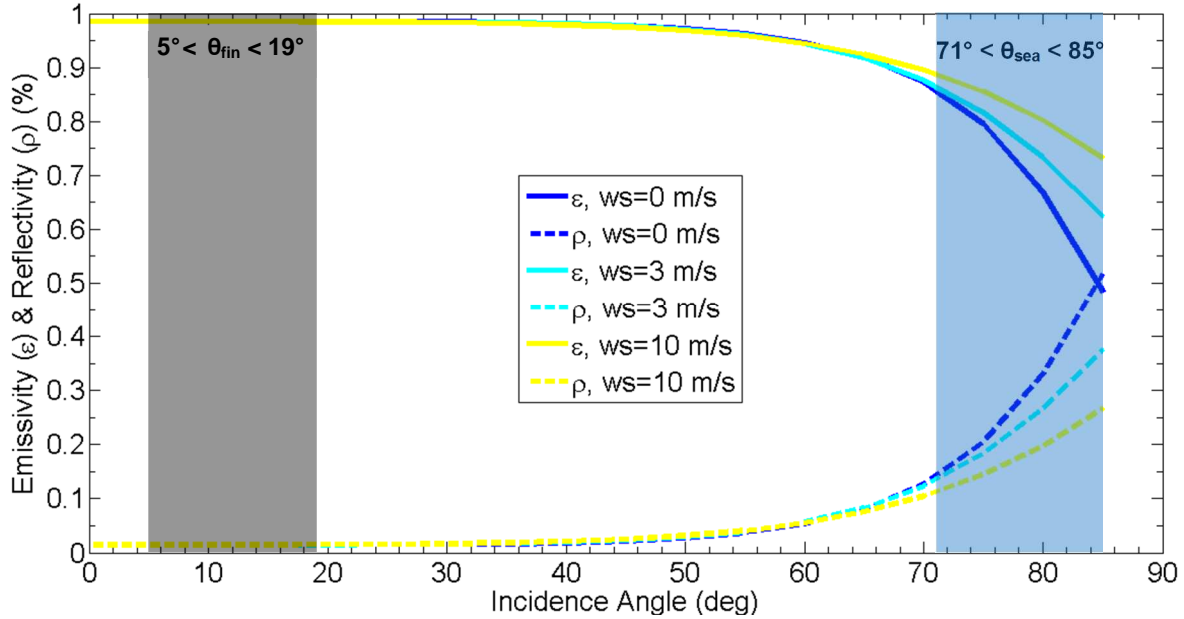


Figure 2. The estimated range of emissivity ( $\epsilon$ ) and reflectivity ( $\rho$ ) from a protruding dorsal fin ( $\theta_{fin}$ ) and the sea surface ( $\theta_{sea}$ )<sup>3</sup>.

## 5. RANGE

The effective range of an infrared camera depends on the camera's resolution, field of view, and the size of the desired target. The camera used for this study has a resolution of 320 x 240 pixels and a 37° horizontal field of view. Figure 3 shows the camera's field of view mapped onto Cartesian coordinates (X-axis facing west, Y-axis facing south)<sup>4</sup>. It can be seen that all fins with a confidence rating of 1 (green square) fall within a 75 meter range. This suggests a maximum distance of 75 meters for identifying killer whale fins with this particular camera and lens geometry. Pixels size is larger on the edge of the field of view due to radial lens distortion.

Whales at distances greater than 100 meters were identified primarily by observing blows. This method is practical to use when the target species and approximate location is already known from other means such as visual observation or hydrophone detection. Blows are distinguished from whales and background noise by tracking the motion through multiple frames. Blows appear and dissipate quickly while whales show steady movement and background noise (such as sun glare) stays relatively fixed.

The smallest blows detected were made up of two pixels at a distance of 162 meters. The purpose of the monitoring system dictates the required resolution. In order to obtain an accurate temperature contrast measurement of a target, there must be at least one pixel not biased low by averaging of the target temperature with the lower temperature of the background. The value for each pixel is an average of the radiation received from the area covered by that pixel. Pixels that only partially cover a target (edge pixels) will therefore return a weighted average of the target and the background radiation based on the percentage of the target covered. Recall that whale fins are approximated as a triangle. In order for at least one pixel of a triangle to not be affected by averaging, a minimum of 9 pixels is required (Figure 4).

As shown in Figure 5, the mean maximum temperature contrast for all identified fins is 1.8 °C. For fins with fewer than 9 pixels the mean is 1.6 °C and for fins with 9 or more pixels the mean is 2.3°C confirming that pixel averaging lowers the maximum apparent temperature for fins with less than 9 pixels. Therefore, only fins with 9 or more pixels will be used for the remainder of this analysis.

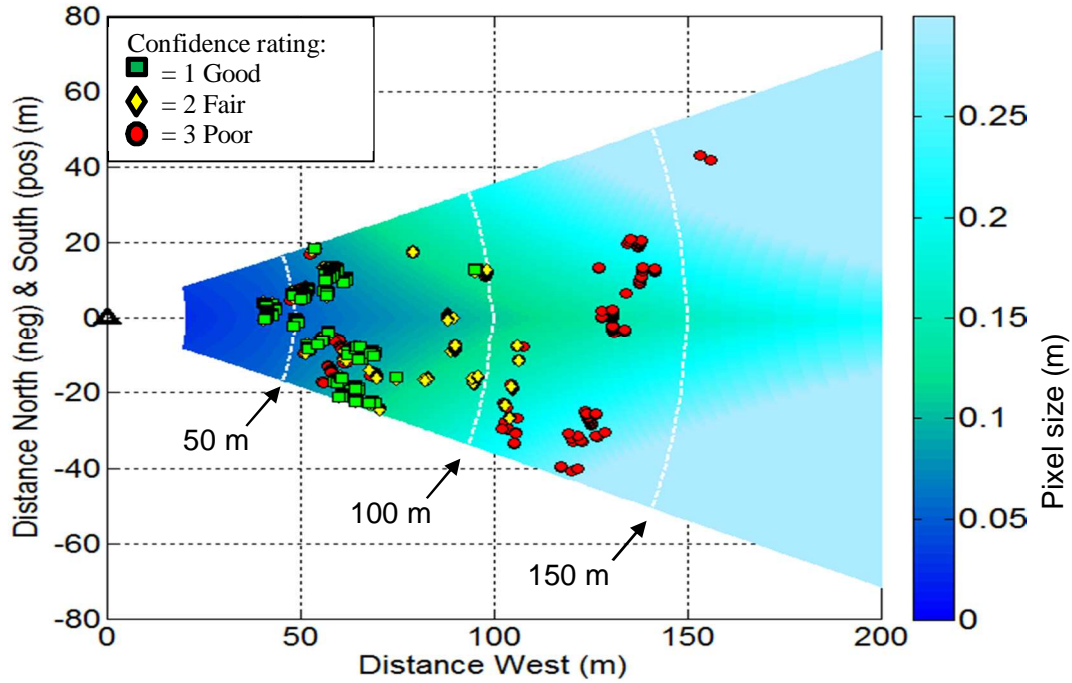


Figure 3. FOV of FLIR A40M camera at Lime Kiln Park in real world coordinates. Axes show distance from camera, the X-axis shows distance west and the Y-axis shows distance south (positive) and north (negative). Contours (white dotted lines) show line of sight distance to camera. Color gradient denotes pixel size (m)

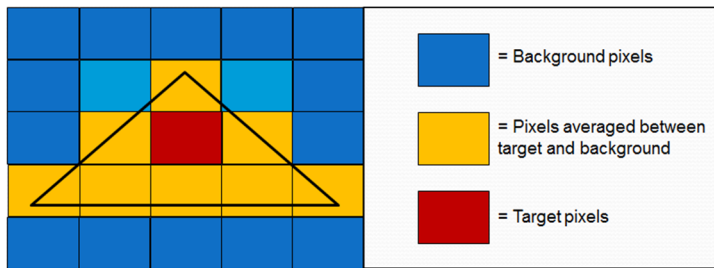


Figure 4. An illustration of the minimum number of pixels (9) required for a triangle target in order to have at least one pixel not affected by pixel averaging.

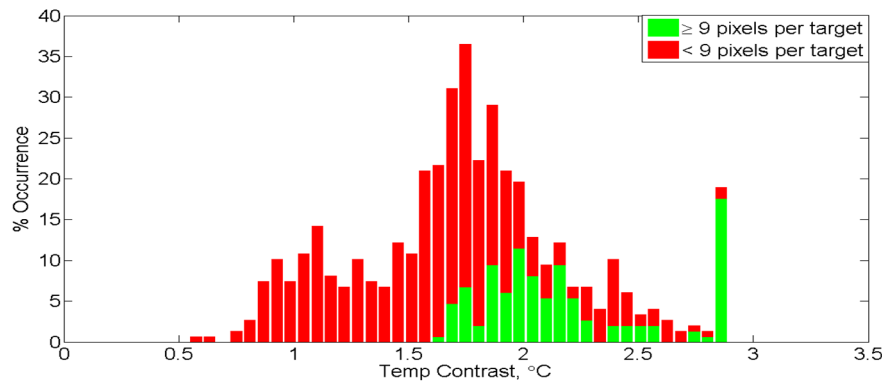


Figure 5. Distribution of maximum temperature contrast between dorsal fin bounding triangles and sea surface. Fins with 9 or more pixels are shown in green and fins with less than 9 pixels are shown in red.

## 6. RESOLUTION

As discussed above, at least 2 pixels per target (PPT) are recommended for the detection of killer whale blows, and at least 9 pixels per target (PPT) are recommended for dorsal fin temperature measurement. These findings, along with target size and working distance, can be used to determine the appropriate infrared camera for a given deployment. Focal plane array resolution is restricted to commercially available sensors. For example, most modern microbolometers have 640 x 480 pixels and the highest resolution currently available is 1024 x 1024 pixels (FLIR SC8000).

To simplify camera selection, initial calculations can be completed considering only the horizontal linear dimensions in the center of the desired field of view. Equation (2) is used to calculate the horizontal width of the camera's field of view for a given horizontal focal plan array (FPA) resolution ( $Px_h$ ), minimum horizontal target size ( $T_h$ ), and horizontal pixels per target ( $PPT_h$ ).

$$W_c(m) = Px_h(\text{pixels}) * \left( \frac{T_h(m)}{PPT_h(\text{pixels})} \right) \quad (2)$$

The calculated width and the estimated distance to the desired target are then used with (3) to calculate the required angular field of view ( $\alpha_c$ ). The required angular field of view is used to select the closest available lens.

$$\alpha_c(\text{degrees}) = 2 * \tan^{-1} \frac{W(m)}{2 * d(m)} \quad (3)$$

Once a camera and lens is selected, a direct linear transformation (DLT) can be used to verify that the approximations are adequate for both horizontal and vertical resolution. To correct for lens distortion, a uniform grid of aluminum foil was attached to white poster board. Since the aluminum foil is highly reflective to infrared radiation and the poster board is not, the apparent temperature contrast can be clearly seen and the lens distortion can be approximated as cubic in radius from the center of the image<sup>3</sup>.

For many applications, multiple camera solutions are required. For example at Admiralty Inlet, the desired minimum target size is 0.5 m (fin size), the desired minimum horizontal width is 250 meters (extent of proposed pilot array), and the desired pixels per target is 9 (high confidence identification of SRKW fins). From (2) it can be seen that even with 1024 x 1024 resolution (the highest resolution currently available) it is not possible to satisfy these requirements with a single camera. Three fixed cameras mounted side by side would provide a 306 meter width, but there would be no added benefit to vertical resolution. Another option is to use a foveal view system. In a foveal view system, one camera is used for detection (2 pixels per target, blow target), and a second camera is used to collect higher resolution images (9 pixels per target, dorsal fin target).

## 7. THE EFFECTS OF INCIDENCE ANGLE

When viewed at incidence angles above 60°, the apparent temperature of the sea surface is expected to be highly dependent on sky temperature ( $T_{sky}$ ) because reflected radiation from the sky begins to dominate over emitted radiation from the sea surface. If  $T_{sky}$  is less than  $T_{sea}$ , as is common on clear days, the sea surface apparent temperature will decrease with increasing incidence angles. Figure 6 shows the apparent temperature change of the sea surface with incidence angle immediately after 6 non-uniformity corrections. As expected, a decrease in apparent sea surface temperature with increasing incidence angles can clearly be seen for incidence angles from 58° (minimum incidence angle recorded, used as reference temp 0 °C) to 76° (max incidence angle recorded). The 4 distinct bumps (66°, 71°, 72°, and 73°) in the 12:33 scene are due to 4 kayakers that passed through the FOV of the camera during this scene, biasing the mean image to a greater extent than the transient from a whale surfacing. The scenes from July 6<sup>th</sup> show a more negative slope between incidence angle and sea surface temperature, suggesting a colder sky temperature that day relative to the 7<sup>th</sup>. For incidence angles greater than 76°, the apparent sea surface temperature increases in the 18:04 and 20:52 scenes. This increase is due to glare from the setting sun. The camera faces west and as the sun approaches the horizon more of the sun's radiation is reflected off the sea surface to the camera. Sunset on July 6<sup>th</sup> was at 21:09 explaining why the glare effect is most pronounced in the 20:52 scene.

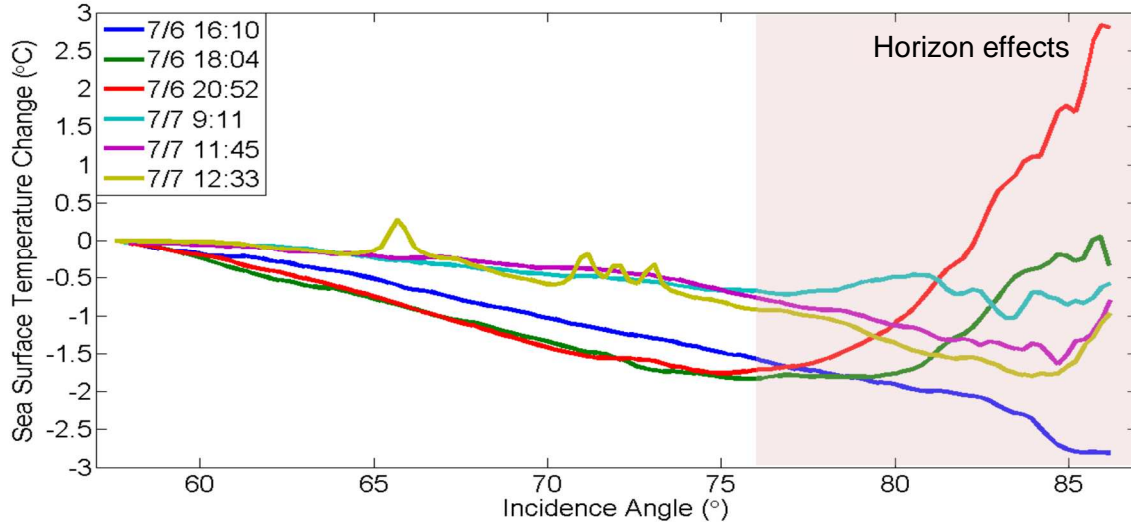


Figure 6. Temperature change of the sea surface relative to the reference bin versus incidence angle for the center column of averaged bins for 6 recordings taken immediately after non-uniform correction (NUC).

The radiance ( $M$ ) measured by an infrared imager is given by

$$M = \varepsilon_{eff}(\theta_{sea})M_{sea}(T_{sea}) + \rho_{eff}(\theta_{sea})M_{sky}(T_{sky}). \quad (4)$$

where  $M_{sea}$  and  $M_{sky}$  are calculated using Planck's function at temperatures  $T_{sea}$  and  $T_{sky}$ ,  $\varepsilon_{eff}$  is the effective sea surface emissivity, and  $\rho_{eff}$  is the effective sea surface reflectivity. For the observations in this study, only a single infrared imager was available so the effective sky temperature was not measured. In order to correlate the observed sea surface temperature change with published values of emissivity it is necessary to approximate the sky temperature. Solving (4) for  $M_{sky}$  at an arbitrary point  $a$  we obtain

$$M_{sky,a}(T_{sky,a}) = \frac{M_a(T_a) - \varepsilon_a M_{sea}(T_{sea})}{(1 - \varepsilon_a)}. \quad (5)$$

The reported sea temperature from the nearest NOAA NDBC buoy (New Dungeness buoy) was 10.9 °C. Since an external blackbody calibration was not performed on the FLIR A40M during the field observations, the infrared footage indicates accurate temperature changes, but not absolute temperatures. In order to determine the absolute temperature, we relate the change in sea surface temperature to the true sea temperature by plotting emissivity versus temperature change and applying a least squares fit. By extrapolation, the temperature change from the true sea surface temperature (0° incidence angle,  $\varepsilon=1$ ) to the reference bin (58° incidence angle,  $\varepsilon=0.95$ ) is found to be approximately -0.2 °C, suggesting an estimated reference temperature of 10.7 °C. Using the estimated reference bin temperature (10.7 °C), the temperature changes from Figure 6, and (5), the estimated sky temperature is found to range between 4.4 and 7.4 °C.

We use this estimate of  $T_{sky}$  to predict the change in fin to sea surface temperature contrast with incidence angle. Figure 7 shows both the observed and expected temperature contrasts as a function of incidence angle. The predicted fin to sea temperature contrasts (dashed lines) were calculated using (4) and the minimum (4.4 °C) and maximum (7.4 °C) estimated sky temperatures. Observed maximum fin to sea temperature contrasts for fins with 9 or more pixels are shown. To obtain the best fit of the observed temperature contrasts, the predicted temperature contrast curves (dashed lines) were adjusted with an empirical offset of 0.4 °C at an incidence angle of 0°. As can be seen, the majority of observed values fall within the predicted envelop at a given incidence angle. The slope of the least squares fit (LSF) curve (solid line) is less steep than the predicted slope for both the minimum and maximum sky temperature (dotted lines). The coefficient of determination ( $R^2$ ) for the LSF is only 0.18 indicating that there is not a significant trend in the data.

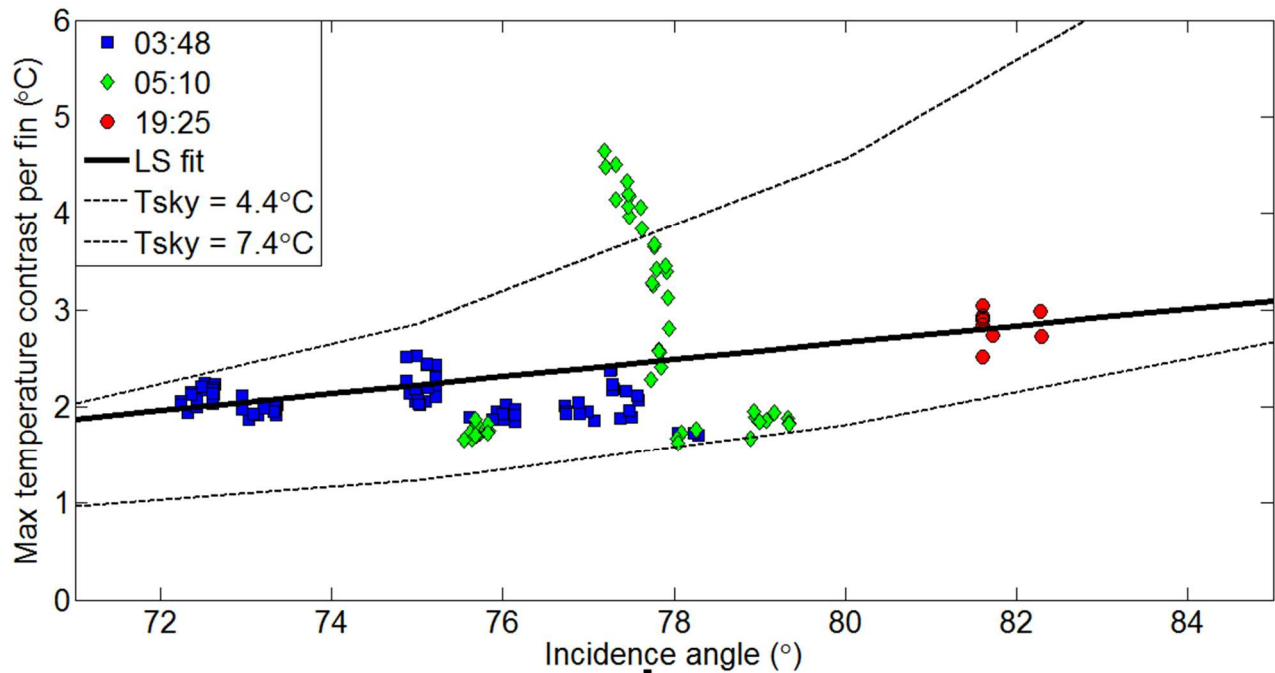


Figure 7. Observed and predicted fin to sea temperature contrast as a function of incidence angle. Predicted values were calculated from the minimum and maximum estimated sky temperatures. Only fins with 9 or more pixels are included.

The fins from the pass at 5:10 have a wide range of observed temperature contrasts, some falling outside the range of values predicted by theory. The standard deviation of temperature contrasts for this pass is 1 °C, nearly an order of magnitude higher than the other two passes (0.17 and 0.15 °C). Although the reasons for this variability are unknown, one possible cause could be reflection of the horizon on the whales' fins since this pass is the only footage collected of whales during the hours of twilight, but future study is required to test this hypothesis.

## 8. INCIDENCE ANGLE DISCUSSION

The apparent temperature contrast between a killer whale dorsal fin and the surround sea surface is a combination of the true temperature contrast and the effects of emissivity. The true temperature contrast is unknown and is expected to vary from fin to fin. Kastings et al.<sup>5</sup> measured the fin to sea temperature contrast of three captive killer whales using a skin-surface thermistor and found that it ranged between 1.4 and 2.2 °C. Since a thermistor was used, these values represent the temperature contrast from the skin-surface of the dorsal fin. When a whale surfaces, the dorsal fin remains covered with a thin film of sea water. Since water is virtually opaque to infrared radiation, the fin temperature measured by an infrared imager is the temperature of the water on the surface of the fin, and is therefore expected to be lower than the fin skin surface temperature. Using an infrared imager, Cuyler et al.<sup>6</sup> measured the fin to sea temperature contrast of free living minke, humpback, and fin whales and found that it ranged between 0.5 and 1.9 °C.

As discussed above, the predicted fin to sea temperature contrast curves fit the observed data best with an empirical offset of 0.4 °C at an incidence angle 0°. This suggests a true fin to sea temperature contrast of 0.4 °C, however there is not a statistically significant trend in the observed data ( $R^2 = 0.18$ ). Also, the slope of the least squares fit curve in Figure 7 is less than the predicted trend suggesting a true temperature contrast greater than 0.4 °C. The apparent temperature of the sea surface varies by as much as 1.7 °C (Figure 6) due to emissivity effects, and the mean observed temperature contrast of fins with 9 or more pixels is only 2.3 °C (Figure 5). Although an accurate estimate of the true fin to sea temperature contrast is not possible with the current data, it can be inferred that emissivity effects explain much of the observed fin to sea temperature contrast.

## 9. AUTOMATED DETECTION

Infrared imagery of marine mammals offers the added benefit of simplifying automated detection. Automated detection using visual imagery relies principally on detected motion. Since the sea surface is in constant motion, this can lead to many false detections. Automated detection using infrared imagery is based on thermal gradients. Since the temperature of the sea surface is nearly uniform in calm conditions, there are fewer false detections. However, in rough seas, the incidence angles to surface waves can give rise to elevated apparent temperature and increasing infrared “clutter”. Basic detection systems for both visual and infrared imagery were tested at Lime Kiln Park. The standard motion detection provided with the Canon VB-C50FSi showed constant detection due to tidal currents and surface waves. By adjusting the sensitivity and creating a mask for waves in the near field of view, the detections could be limited to once every few minutes, however, with these settings, passing whales were not detected in the visual imagery. In summary, motion detection using a visual spectrum camera is likely to result in a high number of false positive detections for this application.

Infrared footage was processed through two phases of automated detection. First, footage was analyzed using the default object recognition functions in MATLAB’s image processing toolbox. Not surprisingly, objects (waves, surface disturbances, boats, birds, etc) were detected in nearly every frame. Next, a simple algorithm was implemented to help distinguish whales from false detections. Thresholds were applied to classify objects as whales based on signal intensity, total area, perimeter, and eccentricity. In addition, neighboring frames are compared to filter false detections that only occurred in single frames.

These thresholds were determined empirically through trial and error. The footage from the July 7<sup>th</sup> pass at 3:48 (longest pass) was analyzed with the automated detection algorithm and false detections were systematically removed by modifying the threshold values. The intensity threshold (60 counts) corresponds to a minimum temperature contrast of 0.6 °C. The area minimum (30 pixels) and maximum (1000 pixels) will vary greatly depending on the distance to the target. The current algorithm is therefore only applicable to surfacing events between 40 and 60 meters (the range of surfacing events from the 3:48 pass). The area threshold removes false detections from very small and very large surface disturbances. Detected surface waves with areas larger than the minimum area threshold frequently appear as long arcs which have large perimeters and eccentricities but small enough areas to be below the maximum area threshold. For these false detections the perimeter (max 200 pixels) and eccentricity (max 0.99) thresholds were added. Objects passing all criteria are identified with a bounding box and range and temperature contrast are displayed. Video 1 shows an example of the output of the developed algorithm and Table 2 summarizes the results of the developed algorithm on the July 7<sup>th</sup> pass at 3:48.

Table 2. Results of the automated detection algorithm on the July 7<sup>th</sup> pass at 3:48.

	Duration of review	Frames to review	Whales detected	False detections
Manual detection	150 seconds	1130	71	-
Automated detection	9 seconds	70	60	42
Percent	6%	6%	85%	-

The automated algorithm shows detection in only 70 frames (6% of the original footage) and accounts for 85% of the surfacing whales identified by manual review. This shows that even a simple algorithm can significantly reduce the footage requiring manual review, while maintaining a high detection rate. A more sophisticated algorithm could be developed to increase the percentage of whales identified and decrease the false detections. By tracking whales through multiple frames, as for some machine vision algorithms, it is conceivable that an automated detection program could be developed using shape and motion classification that would either eliminate or significantly decrease the amount of footage requiring manual review.

## 10. ADVANTAGES OF INFRARED IMAGERY

In this section, the advantages of infrared imagery over visual observation are quantified for use in observing a tidal energy pilot project in northern Admiralty Inlet. Performance data for infrared imagery is not available for all weather conditions because of the limited literature regarding infrared detection of marine mammals. The field observations for

this study were recorded in ideal weather conditions (clear skies, calms seas, and wind speeds below 4 m/s) and cannot provide additional insight. Therefore, it is not possible to construct a full performance gradient model for marine mammal detectability based on meteorological data. After reviewing the underlying physics behind infrared and visual camera performance, pass-fail criteria for detectability are established. These criteria are based on relevant literature from the fields of infrared detection of ground targets, free space optics (FSO), and Civil Aviation. These criteria are then compared to weather conditions at Admiralty Inlet for each hour over the course of a year (2008 is used as a representative year based on availability of data). Although the meteorological data used is specific to Admiralty Inlet, the methodology can be transferred to any location. Meteorological data is compiled from three sources, the Whidbey Island AgWeatherNet Station maintained by Washington State University, the Whidbey Island Naval Air Station (NAS), and NOAA’s National Data Buoy Center station 46088 (New Dungeness, WA).

Table 3 summarizes the benefit of infrared observation over visual observation in Admiralty Inlet, as quantified by the pass-fail criteria and meteorological data from 2008.

Table 3. Summary of the benefits of infrared observation over visual observation. Infrared shows a 28 percentage point (74%) increase over visual.

Parameters	Data Source	Visual		Infrared	
		Criteria	%	Criteria	%
Ambient Light	Field observations (Lime Kiln and Admiralty Inlet)	Between Civil Dawn & Dusk	56%	All hours	100%
Relative Humidity	Stull et al. <sup>7</sup> and Wyatt et al. <sup>8</sup>	All hours	100%	All hours	100%
Fog	Beier & Gemperleing <sup>9</sup>	CAT I fog or below	99%	CAT I fog or below	99%
Sea State	Baldacci et al. <sup>10</sup>	Sea State 2 or below	68%	Sea State 2 or below	68%
<b>Composite</b>		<b>All criteria satisfied</b>	<b>39%</b>	<b>All criteria satisfied</b>	<b>67%</b>

All four of the criteria must be satisfied for each hour to be considered as a pass for the combined percentage. The parameter with the greatest sensitivity is sea state (68%). If detection is possible in sea state 3, the combined results would change to 59% for visual and 95% for infrared (i.e. infrared detection could enable nearly continuous observation). Additional parameters not considered in this evaluation that could influence the system effectiveness include high sky temperature, sun glare, and precipitation.

## 11. CONCLUSIONS

A land-based infrared camera (FLIR Thermovision A40M, 7.5-14µm, 37°HFOV, 320x240 pixels) was used to detect Southern Resident killer whales from Lime Kiln park in Washington State. The primary purpose of this study is to evaluate the efficacy of infrared imagery for monitoring marine mammals at a proposed tidal energy pilot project in northern Admiralty Inlet, Puget Sound. Results from a field study at a nearby site demonstrate the successful detection of killer whales (body, dorsal fin, and blow) during both day and night at ranges from 43 to 162 meters. Whales at distances greater than 100 meters were identified primarily by their blows and suggest a minimum of 2 pixels per target for detection.

The apparent dorsal fin to sea temperature contrast shows dependence on both the number of pixels per target and incidence angle. For a killer whale dorsal fin, at least 9 pixels per target are necessary to minimize the effects of pixel averaging on maximum observed temperature contrast. The apparent fin to sea temperature contrast increases with incidence angle. This increase is shown to be related to the reflection of sky radiation due to increased surface reflectivity at near-grazing angles. Observations are in agreement for predicted increase of fin to sea temperature contrast with incidence angle.

The benefits of infrared imagery include the addition of night-time detection which increases the hours of possible detection. For the case study of Admiralty Inlet, observation time increases by 74% (28% percentage point increase) for infrared-based systems versus visual detection.

The implementation of automated detection is simplified by detecting temperature gradients instead of motion. A simple algorithm is developed that reduced frames requiring review by 94% and identifies 85% of surfacing whales. Further refinement is required to reduce the number of missed detections and false-positives.

## REFERENCES

- [1] National Marine Fisheries Service, "Recovery Plan for Southern Resident Killer Whales (*Orcinus orca*)," National Marine Fisheries Service, Northwest Region (2008).
- [2] Thomson, J., unpublished, (2007).
- [3] Filipiak, M., "Refractive indices (500-3500 cm<sup>-1</sup>) and emissivity (600-3350 cm<sup>-1</sup>) of pure water and seawater," <http://hdl.handle.net/10283/17> (2008).
- [4] Holland, K. T., Holman, R. A., Lippmann, T. C., Stanley, J., and Plant, N., "Practical use of video imagery in nearshore oceanographic field studies," *IEEE Journal of Oceanic Engineering*, 22(1), 81-92 (1997).
- [5] Kasting, N. W., Adderley, S. A., Safford, T., and Hewlett, K. G., "Thermoregulation in beluga (*Delphinapterus leucas*) and killer (*Orcinus orca*) whales," *Physiological Zoology*, 62(3), 687-701 (1989).
- [6] Cuyler, L. C., Wiulsrod, R., and Oritsland, N. A., "Thermal infrared radiation from free living whales," *Marine Mammal Science*, 8(2), 120-134 (1992).
- [7] Stull, V. R., Wyatt, P. J., and Plass, G. N., "The infrared transmittance of carbon dioxide," *Applied Optics*, 3(2), 243-254 (1964).
- [8] Wyatt, P. J., Stull, V. R., and Plass, G. N., "The infrared transmittance of water vapor," *Applied Optics*, 3(2), 229-241 (1964).
- [9] Beier, K., and Gemperlein, H., "Simulation of infrared detection range at fog conditions for enhanced vision systems in civil aviation," *Aerospace Science and Technology*, 8, 63-71 (2004).
- [10] Baldacci, A., Carron, M., and Portunato, N., "Infrared detection of marine mammals," Technical report SR-443, NATO Undersea Research Centre (2005).